Opto-Electronic Advances

Supplementary information

2023, Vol. 6, No. 3

DOI: 10.29026/oea.2023.220018

# Inverse design and realization of an optical cavity-based displacement transducer with arbitrary response

Qianbo Lu[1]*, Qingxiong Xiao[2], Chengxiu Liu[2], Yinan Wang[2], Qixuan Zhu[1], ManZhang Xu[1], Xuewen Wang[1], Xiaoxu Wang[2]* and Wei Huang[1]*

[1]Ningbo Institute of Northwestern Polytechnical University, Frontiers Science Center for Flexible Electronics (FSCFE), MIIT Key Laboratory of Flexible Electronics (KLoFE), Shaanxi Key Laboratory of Flexible Electronics (KLoFE), Institute of Flexible Electronics (IFE), Northwestern Polytechnical University, Xi'an 710072, China; [2]The Key Laboratory of Information Fusion Technology, Ministry of Education, School of Automation, Northwestern Polytechnical University, 127 West Youyi Road, Xi'an 710072, China.

*Correspondence: QB Lu, E-mail: iamqlu@nwpu.edu.cn; XX Wang, E-mail: woyaofly1982@163.com;
W Huang, E-mail: iamwhuang@nwpu.edu.cn

**This file includes:**



Supplementary information for this paper is available at https://doi.org/10.29026/oea.2023.220018

## Section 1: Theoretical model of reflection in condition of anisotropic media

Regarding the reflection by anisotropic stratified systems, we start from Maxwell's equations

$$\begin{gathered}\nabla\times\boldsymbol{E}=-\mathrm{i}\omega\boldsymbol{B}\\ \nabla\times\boldsymbol{H}=\mathrm{i}\omega\boldsymbol{D}\ .\end{gathered}\tag{S1.1}$$

Putting the Cartesian components of electromagnetic-field vectors together in a column, we have two column vectors $\boldsymbol{I}$ and $\boldsymbol{J}$, whose elements are $E_x$, $E_y$, $E_z$, followed by $H_x$, $H_y$, $H_z$, and $D_x$, $D_y$, $D_z$ followed by $B_x$, $B_y$, $B_z$. Then, the matrix form of Eq. (S1.1) can be written as

$$\begin{bmatrix} 0 & 0 & 0 & 0 & -\partial/\partial z & \partial/\partial y\\ 0 & 0 & 0 & \partial/\partial z & 0 & -\partial/\partial x\\ 0 & 0 & 0 & -\partial/\partial y & \partial/\partial x & 0\\ 0 & \partial/\partial z & -\partial/\partial y & 0 & 0 & 0\\ -\partial/\partial z & 0 & \partial/\partial x & 0 & 0 & 0\\ \partial/\partial y & -\partial/\partial x & 0 & 0 & 0 & 0 \end{bmatrix}\begin{bmatrix}E_x\\E_y\\E_z\\H_x\\H_y\\H_z\end{bmatrix}=\mathrm{i}\omega\begin{bmatrix}D_x\\D_y\\D_z\\B_x\\B_y\\B_z\end{bmatrix}$$

$$\Rightarrow \boldsymbol{OI}=\mathrm{i}\omega\boldsymbol{J}\ .\tag{S1.2}$$

The constitutive relation between $\boldsymbol{I}$ and $\boldsymbol{J}$ can be put as the following, in the absence of nonlinear optical effects and dispersion

$$\boldsymbol{J}=\boldsymbol{AI}\ ,\tag{S1.3}$$

where $\boldsymbol{A}$ is the optical matrix, which carries the information about the anisotropic optical properties of the medium

$$\boldsymbol{A}=\begin{bmatrix} \varepsilon_{11} & \varepsilon_{12} & \varepsilon_{13} & \rho_{11} & \rho_{12} & \rho_{13}\\ \varepsilon_{21} & \varepsilon_{22} & \varepsilon_{23} & \rho_{21} & \rho_{22} & \rho_{23}\\ \varepsilon_{31} & \varepsilon_{32} & \varepsilon_{33} & \rho_{31} & \rho_{32} & \rho_{33}\\ \rho_{11} & \rho_{21} & \rho_{31} & \mu_{11} & \mu_{12} & \mu_{13}\\ \rho_{12} & \rho_{22} & \rho_{32} & \mu_{21} & \mu_{22} & \mu_{23}\\ \rho_{13} & \rho_{23} & \rho_{33} & \mu_{31} & \mu_{32} & \mu_{33} \end{bmatrix}=\begin{bmatrix}\boldsymbol{\varepsilon} & \boldsymbol{\rho}\\ \boldsymbol{\rho}' & \boldsymbol{\mu}\end{bmatrix},\tag{S1.4}$$

in which $\boldsymbol{\varepsilon}$, $\boldsymbol{\mu}$ and $\boldsymbol{\rho}$ are the permittivity, permeability, and optical-rotation tensors. Then Eq. (S1.2) converts to the form as

$$\boldsymbol{OI}=\mathrm{i}\omega\boldsymbol{AI}\ .\tag{S1.5}$$

Assume that the light is incident from an isotropic ambient medium onto an investigated stratified structure along the positive $z$-axis, and the coordinate system is shown in Fig. S1. From the symmetry, it is easy to obtain

$$\partial/\partial y=0\ .\tag{S1.6}$$

In addition, it is straightforward to have the spatial dependence along the $x$-axis since all fields should vary in the $x$-direction as $\mathrm{e}^{-\mathrm{i}\zeta x}$

$$\partial/\partial x=-\mathrm{i}\zeta\ ,\tag{S1.7}$$

where $\zeta$ can be expressed by the refractive index $nr_0$ of the ambient and the incident angle $\varphi_0$,

$$\zeta=\frac{nr_i\sin\varphi_0}{\lambda}\ .\tag{S1.8}$$

Substituting Eq. (S1.6) and (S1.7) into Eq. (S1.5), operator $\boldsymbol{O}$ generates two linear homogeneous algebraic equations and four linear homogeneous first-order differential equations, which means the dimension of Eq. (S1.5) can be reduced to a 4 × 4 matrix form

$$\frac{\partial}{\partial z}\begin{bmatrix}E_x\\H_y\\E_y\\-H_x\end{bmatrix}=-\mathrm{i}\omega\begin{bmatrix}\Delta_{11}&\Delta_{12}&\Delta_{13}&\Delta_{14}\\ \Delta_{21}&\Delta_{22}&\Delta_{23}&\Delta_{24}\\ \Delta_{31}&\Delta_{32}&\Delta_{33}&\Delta_{34}\\ \Delta_{41}&\Delta_{42}&\Delta_{43}&\Delta_{44}\end{bmatrix}\begin{bmatrix}E_x\\H_y\\E_y\\-H_x\end{bmatrix}$$

$$\Rightarrow\frac{\partial}{\partial z}\boldsymbol{I}'=-\mathrm{i}\omega\boldsymbol{\Delta}\boldsymbol{I}'\ .\tag{S1.9}$$

Herein $\boldsymbol{I}'$ is the 4 × 1 generalized field vector and $\boldsymbol{\Delta}$ is a 4 × 4 differential propagation matrix, whose elements are functions of the elements of the optical matrix $\boldsymbol{A}$[S1]

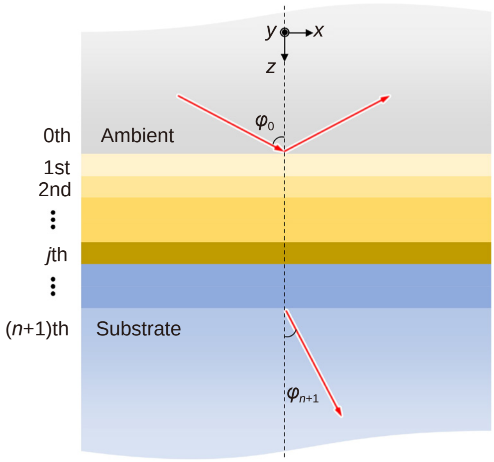


**Fig. S1 | Schematic diagram of the reflection and transmission of a plane wave by a stratified system.**

$$
\begin{aligned}
\Delta_{11} &= \rho_{12} + (\rho_{32}+\eta)(\rho_{13}\rho_{33} - \varepsilon_{31}\mu_{33}) / (\varepsilon_{33}\mu_{33} - \rho_{33}\rho_{33}) + \mu_{23}(\rho_{33}\varepsilon_{31} - \varepsilon_{33}\rho_{13}) / (\varepsilon_{33}\mu_{33} - \rho_{33}\rho_{33}) \\
\Delta_{12} &= \mu_{22} + (\rho_{32}+\eta)(\mu_{23}\rho_{33} - (\rho_{23}+\eta)\mu_{33}) / (\varepsilon_{33}\mu_{33} - \rho_{33}\rho_{33}) + \mu_{23}((\rho_{32}+\eta)\rho_{33} - \varepsilon_{33}\mu_{23}) / (\varepsilon_{33}\mu_{33} - \rho_{33}\rho_{33}) \\
\Delta_{13} &= \rho_{22} + (\rho_{32}+\eta)((\rho_{23}-\eta)\rho_{33} - \varepsilon_{32}\mu_{33}) / (\varepsilon_{33}\mu_{33} - \rho_{33}\rho_{33}) + \mu_{23}(\rho_{33}\varepsilon_{32} - (\rho_{23}-\eta)\varepsilon_{33}) / (\varepsilon_{33}\mu_{33} - \rho_{33}\rho_{33}) \\
\Delta_{14} &= -\mu_{21} - (\rho_{32}+\eta)(\mu_{31}\rho_{33} - \rho_{31}\mu_{33}) / (\varepsilon_{33}\mu_{33} - \rho_{33}\rho_{33}) - \mu_{23}(\rho_{33}\rho_{31} - \varepsilon_{33}\mu_{31}) / (\varepsilon_{33}\mu_{33} - \rho_{33}\rho_{33}) \\
\Delta_{21} &= \varepsilon_{11} + \varepsilon_{13}(\rho_{13}\rho_{33} - \varepsilon_{31}\mu_{33}) / (\varepsilon_{33}\mu_{33} - \rho_{33}\rho_{33}) + \rho_{13}(\rho_{33}\varepsilon_{31} - \varepsilon_{33}\rho_{13}) / (\varepsilon_{33}\mu_{33} - \rho_{33}\rho_{33}) \\
\Delta_{22} &= \rho_{12} + \varepsilon_{13}(\mu_{23}\rho_{33} - (\rho_{23}+\eta)\mu_{33}) / (\varepsilon_{33}\mu_{33} - \rho_{33}\rho_{33}) + \rho_{13}((\rho_{32}+\eta)\rho_{33} - \varepsilon_{33}\mu_{23}) / (\varepsilon_{33}\mu_{33} - \rho_{33}\rho_{33}) \\
\Delta_{23} &= \varepsilon_{12} + \varepsilon_{13}((\rho_{23}-\eta)\rho_{33} - \varepsilon_{32}\mu_{33}) / (\varepsilon_{33}\mu_{33} - \rho_{33}\rho_{33}) + \rho_{13}(\rho_{33}\varepsilon_{32} - (\rho_{23}-\eta)\varepsilon_{33}) / (\varepsilon_{33}\mu_{33} - \rho_{33}\rho_{33}) \\
\Delta_{24} &= -\rho_{11} - \varepsilon_{13}(\mu_{31}\rho_{33} - \rho_{31}\mu_{33}) / (\varepsilon_{33}\mu_{33} - \rho_{33}\rho_{33}) - \rho_{13}(\rho_{33}\rho_{31} - \varepsilon_{33}\mu_{31}) / (\varepsilon_{33}\mu_{33} - \rho_{33}\rho_{33}) \\
\Delta_{31} &= -\rho_{11} - \rho_{31}(\rho_{13}\rho_{33} - \varepsilon_{31}\mu_{33}) / (\varepsilon_{33}\mu_{33} - \rho_{33}\rho_{33}) - \mu_{13}(\rho_{33}\varepsilon_{31} - \varepsilon_{33}\rho_{13}) / (\varepsilon_{33}\mu_{33} - \rho_{33}\rho_{33}) \\
\Delta_{32} &= -\mu_{12} - \rho_{31}(\mu_{23}\rho_{33} - (\rho_{23}+\eta)\mu_{33}) / (\varepsilon_{33}\mu_{33} - \rho_{33}\rho_{33}) - \mu_{13}((\rho_{32}+\eta)\rho_{33} - \varepsilon_{33}\mu_{23}) / (\varepsilon_{33}\mu_{33} - \rho_{33}\rho_{33}) \\
\Delta_{33} &= -\rho_{21} - \rho_{31}((\rho_{23}-\eta)\rho_{33} - \varepsilon_{32}\mu_{33}) / (\varepsilon_{33}\mu_{33} - \rho_{33}\rho_{33}) - \mu_{13}(\rho_{33}\varepsilon_{32} - (\rho_{23}-\eta)\varepsilon_{33}) / (\varepsilon_{33}\mu_{33} - \rho_{33}\rho_{33}) \\
\Delta_{34} &= \mu_{11} + \rho_{31}(\mu_{31}\rho_{33} - \rho_{31}\mu_{33}) / (\varepsilon_{33}\mu_{33} - \rho_{33}\rho_{33}) + \mu_{13}(\rho_{33}\varepsilon_{31} - \varepsilon_{33}\rho_{13}) / (\varepsilon_{33}\mu_{33} - \rho_{33}\rho_{33}) \\
\Delta_{41} &= \varepsilon_{21} + \varepsilon_{23}(\rho_{13}\rho_{33} - \varepsilon_{31}\mu_{33}) / (\varepsilon_{33}\mu_{33} - \rho_{33}\rho_{33}) + (\rho_{23}-\eta)(\rho_{33}\varepsilon_{31} - \varepsilon_{33}\rho_{13}) / (\varepsilon_{33}\mu_{33} - \rho_{33}\rho_{33}) \\
\Delta_{42} &= \rho_{22} + \varepsilon_{23}(\mu_{23}\rho_{33} - (\rho_{23}+\eta)\mu_{33}) / (\varepsilon_{33}\mu_{33} - \rho_{33}\rho_{33}) + (\rho_{23}-\eta)((\rho_{32}+\eta)\rho_{33} - \varepsilon_{33}\mu_{23}) / (\varepsilon_{33}\mu_{33} - \rho_{33}\rho_{33}) \\
\Delta_{43} &= \varepsilon_{22} + \varepsilon_{23}((\rho_{23}-\eta)\rho_{33} - \varepsilon_{32}\mu_{33}) / (\varepsilon_{33}\mu_{33} - \rho_{33}\rho_{33}) + (\rho_{23}-\eta)(\rho_{33}\varepsilon_{32} - (\rho_{23}-\eta)\varepsilon_{33}) / (\varepsilon_{33}\mu_{33} - \rho_{33}\rho_{33}) \\
\Delta_{44} &= \rho_{21} + \varepsilon_{23}(\mu_{31}\rho_{33} - \rho_{31}\mu_{33}) / (\varepsilon_{33}\mu_{33} - \rho_{33}\rho_{33}) + (\rho_{23}-\eta)(\rho_{33}\varepsilon_{31} - \varepsilon_{33}\rho_{13}) / (\varepsilon_{33}\mu_{33} - \rho_{33}\rho_{33}) \ ,
\end{aligned}
\tag{S1.10}
$$

where $\eta = \zeta / \omega$. Regarding certain anisotropic media with a known $\boldsymbol{\Delta}$, the generalized field vector is specified by Eq. (S1.9). Even though the expression of $\boldsymbol{\Delta}$ seems to be too complicated, it can always be reduced to a relatively simple form. For example, the differential propagation matrix for an orthorhombic crystal with its principal axes parallel to the $x$, $y$, $z$-axes, which is a typical anisotropic medium[S2], has the following form

$$
\boldsymbol{\Delta} = \begin{bmatrix} 0 & \mu_{22} - (\eta^2/\varepsilon_{33}) & 0 & 0 \\ \varepsilon_{11} & 0 & 0 & 0 \\ 0 & 0 & 0 & \mu_{11} \\ 0 & 0 & \varepsilon_{22} - (\eta^2/\mu_{33}) & 0 \end{bmatrix} . \tag{S1.11}
$$

In the general case, Eq. (S1.9) does not have an analytical solution because the optical matrix $\boldsymbol{A}$ is an arbitrary function of $z$. Usually, we can subdivide the anisotropic medium into parts with a sufficiently thin length of $h$, whose optical matrix is independent of $z$. This yields the integration of Eq. (S1.9) as

$$
\boldsymbol{\Gamma}'(z+h) = \mathrm{e}^{-\mathrm{i}\omega h \Delta} \boldsymbol{\Gamma}'(z) \ , \tag{S1.12}
$$

in which the exponential term can be Taylor expanded. Eq. (S1.13) describes a linear relation between the generalized field vectors at two different positions along the $z$-axis, separated by a distance of $h$. This equation has four particular plane-wave solutions of the form

$$\boldsymbol{I}'(z) = \boldsymbol{I}'_k(0)\,\mathrm{e}^{-\mathrm{i}\omega q_k z}, \qquad k = 1,\ 2,\ 3,\ 4 \tag{S1.13}$$

wherein $q_k$ equals the component of the propagation vector of the plane wave along the $z$-axis. $q_k$ have four values, which are the roots of the quartic polynomial equation

$$\det\left[\omega\boldsymbol{\Delta} - q\boldsymbol{E}\right] = 0\ , \tag{S1.14}$$

where $\boldsymbol{E}$ is the $4 \times 4$ identity matrix.

By using Eq. (S1.12), we can obtain the field vector relation between two parallel positions along the $z$-axis, and the calculation involving a certain distance $d$ can be realized by the accumulation of thin thickness $h$, written as

$$\boldsymbol{I}'(z+d) = \mathrm{e}^{-\mathrm{i}\omega h_m \Delta_{z+d-h_m}} \cdots \mathrm{e}^{-\mathrm{i}\omega h_2 \Delta_{z+h_1}} \mathrm{e}^{-\mathrm{i}\omega h_1 \Delta_z} \boldsymbol{I}'(z)\ ,$$
$$d = \sum_{i=1}^{m} h_i\ , \tag{S1.15}$$

where $\boldsymbol{\Delta}_{z+h_i}$ denotes the differential propagation matrix of the medium at the position of $z + h_i$. Eq. S1.15 can be used to calculate the field vector numerically, and then the reflection and transmission properties with increased accuracy of the division length.

## Section 2: Self-built fitness function setting and corresponding values

The evaluation factors of the self-built fitness function are shown in the main text. Herein we give the detailed function and its values.

Regarding the factor of the absolute intensity and contrast, we combine them together, then obtain

$$f_1 + f_2 = 1 - \left(\frac{I_{\max}}{2} + \frac{I_{\max} - I_{\min}}{2\left(I_{\max} + I_{\min}\right)}\right)\ . \tag{S2.1}$$

It means that the weight factors $w_1$ and $w_2$ mentioned in the main text are both 0.5.

Regarding the factor of the linearity, we have

$$f_3 = 0.1 \times \left(2\left(1 - R_{L_1}^2\right) + \frac{SSE_{L_1}}{2} + 2\left(1 - R_{L_2}^2\right) + \frac{SSE_{L_2}}{2}\right) / \left(I_{\max} - I_{\min}\right)\ , \tag{S2.2}$$

where $R_{L1}{}^2$ and $SSE_{L1}$ denote the R-squared value and sum of squares due to error of the part $L_1$ shown in Fig. 4 in the main text, and $R_{L2}{}^2$ and $SSE_{L2}$ denote those of the part $L_2$. The scale factor of 0.1 and the weight factors 2 and 0.5 contained in the numerator are set to adjust $f_3$ to a value comparable to $f_1$ and $f_2$. In addition, the denominator is used to normalize the factor.

Regarding the factor of the symmetry, we have

$$f_4 = \left|\max\left\{L_1, L_2\right\} - \frac{\lambda}{2}\right|. \tag{S2.3}$$

Actually, the values of the weight factors are taken based on the probability distribution of each evaluation factor. As shown in Fig. S2, the settings defined in Eqs. (S2.1–S2.3) help to make each evaluation factor has a feasible weight in the overall fitness value. The absolute intensity, contrast ($f_1$) and linearity ($f_2$) are our major concerns, which are in the same order of magnitude. It is easy to adjust the factors in terms of different design goals. For example, the asymmetry condition expressed in Eq. (S2.3) can be readily changed to the symmetry condition by changing the component of $\lambda/2$ to $\lambda/4$.

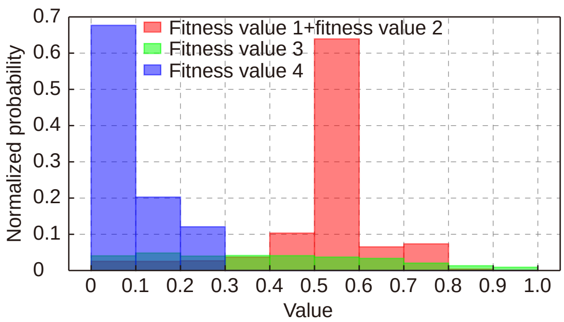


**Fig. S2 | Histogram of the distribution of each evaluation factor for Ge/17 nm/Ag up-case setting.**

## Section 3: Material library

Here we give a detailed list of the materials used in the inverse design. The simple substances, normal materials, and whole materials are listed in Table S1, wherein the gold base color represents the simple substances, the orange color represents the normal materials, and the blue color represents whole materials. Although the table only lists the

**Table S1 | Detailed list of materials**

| Index | Material | *nr*@850 nm | Index | Material | *nr*@850 nm | Index | Material | *nr*@850 nm |
|---|---|---|---|---|---|---|---|---|
| 1 | Ag | 0.1000 – 5.5840i[S3] | 47 | $Ta_2O_5$ | 2.1500 – 0i[S4] | 93 | $KTaO_3$ | 2.1877 – 0i[S5] |
| 2 | Al | 2.2049 – 7.1881i[S6] | 48 | TiC | 3.5360 – 3.1102i[S7] | 94 | $LaF_3$ | 1.5799 – 0.0005i[S8] |
| 3 | Au | 0.2700 – 5.1100i[S9] | 49 | TiN | 1.8693 – 3.8796i[S7] | 95 | $LiB_3O_5$ | 1.5690 – 0i[S10] |
| 4 | Be | 3.4066 – 3.4712i[S11] | 50 | $TiO_2$ | 2.0888 – 0i[S12] | 96 | LiBr | 1.7801 – 0i[S13] |
| 5 | Bi | 0.2658 – 6.8027i[S14] | 51 | W | 3.3950 – 2.8610i[S15] | 97 | LiCl | 1.6594 – 0i[S13] |
| 6 | Co | 0.7517 – 8.1384i[S14] | 52 | ZnO | 1.7535 – 0.0273i[S16] | 98 | LiF | 1.3885 – 0i[S13] |
| 7 | Cr | 3.2408 – 3.4963i[S17] | 53 | ZnSe | 2.5005 – 0i[S18] | 99 | LiI | 1.9518 – 0i[S13] |
| 8 | Cs | 0.2960 – 1.8867i[S19] | 54 | Zr | 2.6933 – 1.9604i[S20] | 100 | $LiIO_3$ | 1.8637 – 0i[S21] |
| 9 | Cu | 0.2763 – 5.4197i[S9] | 55 | $ZrO_2$ | 2.1320 – 0i[S22] | 101 | $MgAl_2O_4$ | 1.7062 – 0i[S23] |
| 10 | Fe | 4.7792 – 11.2036i[S14] | 56 | AgCl | 2.0309 – 0i[S24] | 102 | $MgH_2$ | 2.4017 – 1.0718i[S20] |
| 11 | Ge | 4.8900 – 0.8200i[S25] | 57 | AlAs | 2.9944 – 0.0001i[S26] | 103 | $MoO_3$ | 2.0613 – 0.1109i[S27] |
| 12 | In | 1.9574 – 6.9328i[S28] | 58 | $As_2S_3$ | 2.5067 – 0i[S29] | 104 | $MoS_2$ | 3.2814 – 0.0988i[S30] |
| 13 | Mg | 0.9159 – 8.2340i[S31] | 59 | $BaB_2O_4$ | 1.6599 – 0i[S32] | 105 | $MoSe_2$ | 4.8555 – 0i[S33] |
| 14 | Mn | 2.8872 – 4.0913i[S17] | 60 | $BaF_2$ | 1.4698 – 0i[S34] | 106 | $MoTe_2$ | 4.5868 – 1.1058i[S35] |
| 15 | Mo | 2.0632 – 12.2762i[S14] | 61 | BeO | 1.7117 – 0i[S23] | 107 | NaBr | 1.6277 – 0i[S13] |
| 16 | Ni | 2.8589 – 9.6266i[S14] | 62 | $Bi_2Se_3$ | 4.3197 – 0.9517i[S36] | 108 | NaCl | 1.5430 – 0i[S37] |
| 17 | Pt | 0.6247 – 8.6439i[S14] | 63 | $BiB_3O_6$ | 1.7638 – 0i[S38] | 109 | NaI | 1.7531 – 0i[S13] |
| 18 | Si | 3.6360 – 0.0035i[S39] | 64 | $BiFeO_3$ | 2.8161 – 0i[S40] | 110 | Ne | 1.0001 – 0i[S41] |
| 19 | Sn | 2.6600 – 6.9800i[S42] | 65 | Ca | 0.3863 – 4.0166i[S28] | 111 | $NH_4H_2PO_4$ | 1.5137 – 0i[S43] |
| 20 | Ta | 0.9823 – 7.7769i[S14] | 66 | $CaCO_3$ | 1.6471 – 0i[S44] | 112 | Pb | 1.2089 – 8.1916i[S14] |
| 21 | Te | 4.4088 – 1.3583i[S45] | 67 | $CaMoO_4$ | 1.9659 – 0i[S46] | 113 | $PbF_2$ | 1.7465 – 0i[S47] |
| 22 | Ti | 0.3527 – 7.2847i[S14] | 68 | $CeF_3$ | 1.6222 – 0.0023i[S8] | 114 | $PbMoO_4$ | 2.3270 – 0i[S48] |
| 23 | V | 0.2787 – 7.6393i[S14] | 69 | $CO_2$ | 1.0004 – 0i[S49] | 115 | $PbTiO_3$ | 2.6009 – 0i[S50] |
| 24 | Zn | 1.9409 – 7.5258i[S14] | 70 | $CS_2$ | 1.6023 – 0i[S51] | 116 | Rb | 0.1019 – 2.2240i[S19] |
| 25 | $SiO_2$ | 1.4688 – 0i[S52] | 71 | CsCl | 1.6292 – 0i[S13] | 117 | RbBr | 1.5414 – 0i[S13] |
| 26 | BK7 | 1.5100 – 0i[S53] | 72 | CsF | 1.4734 – 0i[S13] | 118 | RbCl | 1.4836 – 0i[S13] |
| 27 | BF33 | 1.4660 – 0i[S54] | 73 | CsI | 1.7634 – 0i[S13] | 119 | RbF | 1.3931 – 0i[S13] |
| 28 | AlN | 2.1365 – 0i[S55] | 74 | $CsLiB_6O_{10}$ | 1.4885 – 0i[S56] | 120 | RbI | 1.6285 – 0i[S13] |
| 29 | BN | 2.0952 – 0i[S57] | 75 | CuCl | 1.9364 – 0i[S58] | 121 | $Sc_2O_3$ | 1.9798 – 0i[S59] |
| 30 | C | 2.2689 – 0.7711i[S60] | 76 | $CuGaS_2$ | 2.5784 – 0i[S61] | 122 | $SF_6$ | 1.0007 – 0i[S62] |
| 31 | $CaF_2$ | 1.4300 – 0i[S63] | 77 | $Fe_3O_4$ | 2.2360 – 0.1550i[S64] | 123 | $SrF_2$ | 1.4824 – 0.0048i[S65] |
| 32 | $CaWO_4$ | 1.8998 – 0i[S46] | 78 | GaS | 2.6503 – 0i[S66] | 124 | $SrTiO_3$ | 2.3340 – 0i[S67] |
| 33 | CdS | 2.2961 – 0i[S68] | 79 | GaSb | 4.3310 – 0.3228i[S69] | 125 | $TeO_2$ | 2.2204 – 0i[S70] |
| 34 | CdSe | 2.4608 – 0.0782i[S71] | 80 | $HfO_2$ | 1.8848 – 0i[S72] | 126 | TiH2 | 2.5385 – 3.0272i[S20] |
| 35 | CdTe | 2.8802 – 0.0108i[S68] | 81 | Hg | 3.1380 – 6.3954i[S73] | 127 | TlBr | 2.4752 – 0i[S23] |
| 36 | $Fe_2O_3$ | 2.8240 – 0.0270i[S64] | 82 | $HgGa_2S_4$ | 2.5128 – 0i[S74] | 128 | VC | 3.3864 – 2.9106i[S75] |
| 37 | GaAs | 3.5708 – 0.0243i[S76] | 83 | HgS | 2.7521 – 0i[S77] | 129 | VN | 2.7560 – 2.9619i[S75] |
| 38 | GaN | 2.2400 – 0.0500i[S78] | 84 | InP | 3.4492 – 0.1766i[S79] | 130 | $WS_2$ | 3.0060 – 0.0048i[S80] |
| 39 | $GeO_2$ | 1.5680 – 0i[S25] | 85 | InSb | 4.3900 – 0.4100i[S81] | 131 | $WSe_2$ | 4.3531 – 0.1800i[S82] |
| 40 | Li | 0.3081 – 4.0241i[S83] | 86 | K | 0.0404 – 2.5251i[S84] | 132 | $Y_2O_3$ | 1.9087 – 0i[S85] |
| 41 | $MgF_2$ | 1.4190 – 0.0004i[S8] | 87 | KBr | 1.5475 – 0i[S13] | 133 | $Y_3Al_5O_{12}$ | 1.8198 – 0i[S86] |
| 42 | MgO | 1.7262 – 0i[S87] | 88 | KCl | 1.4820 – 0i[S13] | 134 | $YbF_3$ | 1.4900 – 0i[S88] |
| 43 | NaF | 1.3223 – 0i[S13] | 89 | KF | 1.3594 – 0i[S13] | 135 | $YLiF_4$ | 1.4497 – 0i[S89] |
| 44 | PbSe | 5.3211 – 1.4775i[S90] | 90 | $KH_2PO_4$ | 1.5000 – 0i[S43] | 136 | $YVO_4$ | 1.9681 – 0i[S91] |
| 45 | $Si_3N_4$ | 2.0211 – 0i[S92] | 91 | KI | 1.6457 – 0i[S13] | | | |
| 46 | SiC | 3.2998 – 0.1392i[S93] | 92 | $KNbO_3$ | 2.1348 – 0i[S94] | | | |

complex refractive index at 850 nm, we have established the database for a wide range of wavelengths, covering the commonly used wavelengths.

## References


S1. Vanasse GA, Stair AT Jr, Baker DJ. *Aspen International Conference on Fourier Spectroscopy*, *1970* (Air Force Cambridge Research Labs Hanscom AFB MA, 1971).

S2. Berreman DW. Optics in stratified and anisotropic media: 4 × 4-matrix formulation. *J Opt Soc Am* **62**, 502–510 (1972).

S3. Ciesielski A, Skowronski L, Trzcinski M, Szoplik T. Controlling the optical parameters of self-assembled silver films with wetting layers and annealing. *Appl Surf Sci* **421**, 349–356 (2017).

S4. Rodríguez-de Marcos LV, Larruquert JI, Méndez JA, Aznárez JA. Self-consistent optical constants of $SiO_2$ and $Ta_2O_5$ films. *Opt Mater Express* **6**, 3622–3637 (2016).

S5. Fujii Y, Sakudo T. Dielectric and optical properties of $KTaO_3$. *J Phys Soc Jpn* **41**, 888–893 (1976).

S6. McPeak KM, Jayanti SV, Kress SJP, Meyer S, Iotti S et al. Plasmonic films can easily be better: rules and recipes. *ACS Photonics* **2**, 326–333 (2015).

S7. Pflüger J, Fink J, Weber W, Bohnen KP, Crecelius G. Dielectric properties of $TiC_x$, $TiN_x$, $VC_x$, and $VN_x$ from 1.5 to 40 eV determined by electron-energy-loss spectroscopy. *Phys Rev B* **30**, 1155–1163 (1984).

S8. Rodríguez-de Marcos LV, Larruquert JI, Méndez JA, Aznárez JA. Self-consistent optical constants of $MgF_2$, $LaF_3$, and $CeF_3$ films. *Opt Mater Express* **7**, 989–1006 (2017).

S9. Johnson PB, Christy RW. Optical constants of the noble metals. *Phys Rev B* **6**, 4370–4379 (1972).

S10. Chen CT, Wu YC, Jiang AD, Wu BC, You GM et al. New nonlinear-optical crystal: $LiB_3O_5$. *J Opt Soc Am B* **6**, 616–621 (1989).

S11. Rakić AD, Djurišić AB, Elazar JM, Majewski ML. Optical properties of metallic films for vertical-cavity optoelectronic devices. *Appl Opt* **37**, 5271–5283 (1998).

S12. Sarkar S, Gupta V, Kumar M, Schubert J, Probst PT et al. Hybridized guided-mode resonances via colloidal plasmonic self-assembled grating. *ACS Appl Mater Interfaces* **11**, 13752–13760 (2019).

S13. Li HH. Refractive index of alkali halides and its wavelength and temperature derivatives. *J Phys Chem Ref Data* **5**, 329–528 (1976).

S14. Werner WSM, Glantschnig K, Ambrosch-Draxl C. Optical constants and inelastic electron-scattering data for 17 elemental metals. *J Phys Chem Ref Data* **38**, 1013–1092 (2009).

S15. Weaver JH, Olson CG, Lynch DW. Optical-properties of crystalline tungsten. *Phys Rev B* **12**, 1293–1297 (1975).

S16. Aguilar O, de Castro S, Godoy MPF, Dias MRS. Optoelectronic characterization of $Zn_{1-x}Cd_xO$ thin films as an alternative to photonic crystals in organic solar cells. *Opt Mater Express* **9**, 3638–3648 (2019).

S17. Johnson PB, Christy RW. Optical constants of transition metals: Ti, V, Cr, Mn, Fe, Co, Ni, and Pd. *Phys Rev B* **9**, 5056–5070 (1974).

S18. Marple DTF. Refractive index of ZnSe, ZnTe, and CdTe. *J Appl Phys* **35**, 539–542 (1964).

S19. Smith NV. Optical constants of rubidium and cesium from 0.5 to 4.0 eV. *Phys Rev B* **2**, 2840–2848 (1970).

S20. Palm KJ, Murray JB, Narayan TC, Munday JN. Dynamic optical properties of metal hydrides. *ACS Photonics* **5**, 4677–4686 (2018).

S21. Choy MM, Byer RL. Accurate second-order susceptibility measurements of visible and infrared nonlinear crystals. *Phys Rev B* **14**, 1693–1706 (1976).

S22. Wood DL, Nassau K. Refractive index of cubic zirconia stabilized with yttria. *Appl Opt* **21**, 2978–2981 (1982).

S23. Palik ED. *Handbook of Optical Constants of Solids* Vol. 3 (Academic Press, San Diego, 1998).

S24. Tilton LW, Plyler EK, Stephens RE. Refractive index of silver chloride for visible and infra-red radiant energy. *J Opt Soc Am* **40**, 540–543 (1950).

S25. Nunley TN, Fernando NS, Samarasingha N, Moya JM, Nelson CM et al. Optical constants of germanium and thermally grown germanium dioxide from 0.5 to 6.6 eV via a multisample ellipsometry investigation. *J Vac Sci Technol B* **34**, 061205 (2016).

S26. Rakić AD, Majewski ML. Modeling the optical dielectric function of GaAs and AlAs: extension of Adachi's model. *J Appl Phys* **80**, 5909–5914 (1996).

S27. Vos MFJ, Macco B, Thissen NFW, Bol AA, Kessels WMM. Atomic layer deposition of molybdenum oxide from $(N^tBu)_2(NMe_2)_2Mo$ and $O_2$ plasma. *J Vac Sci Technol A* **34**, 01A103 (2016).

S28. Mathewson AG, Myers HP. Absolute values of the optical constants of some pure metals. *Phys Scr* **4**, 291–292 (1971).

S29. Rodney WS, Malitson IH, King TA. Refractive index of arsenic trisulfide. *J Opt Soc Am* **48**, 633–636 (1958).

S30. Islam KM, Synowicki R, Ismael T, Oguntoye I, Grinalds N et al. In‐plane and out‐of‐plane optical properties of monolayer, few‐layer, and thin‐film $MoS_2$ from 190 to 1700 nm and their application in photonic device design. *Adv Photonics Res* **2**, 2000180 (2021).

S31. Hagemann HJ, Gudat W, Kunz C. Optical constants from the far infrared to the x-ray region: Mg, Al, Cu, Ag, Au, Bi, C, and $Al_2O_3$. *J Opt Soc Am* **65**, 742–744 (1975).

S32. Eimerl D, Davis L, Velsko S, Graham EK, Zalkin A. Optical, mechanical, and thermal properties of barium borate. *J Appl Phys* **62**, 1968–1983 (1987).

S33. Hsu C, Frisenda R, Schmidt R, Arora A, de Vasconcellos SM et al. Thickness‐dependent refractive index of 1L, 2L, and 3L $MoS_2$, $MoSe_2$, $WS_2$, and $WSe_2$. *Adv Opt Mater* **7**, 1900239 (2019).

S34. Malitson IH. Refractive properties of barium fluoride. *J Opt Soc Am* **54**, 628–632 (1964).

S35. Beal AR, Hughes HP. Kramers-kronig analysis of the reflectivity spectra of 2H-$MoS_2$, 2H-$MoSe_2$ and 2H-$MoTe_2$. *J Phys C Solid State Phys* **12**, 881–890 (1979).

S36. Fang MS, Wang ZY, Gu HG, Tong MY, Song BK et al. Layer-dependent dielectric permittivity of topological insulator $Bi_2Se_3$ thin films. *Appl Surf Sci* **509**, 144822 (2020).
S37. Querry MR. *Optical Constants of Minerals and other Materials from the Millimeter to the Ultraviolet* (1987).
S38. Umemura N, Miyata K, Kato K. New data on the optical properties of $BiB_3O_6$. *Opt Mater* **30**, 532–534 (2007).
S39. Schinke C, Peest PC, Schmidt J, Brendel R, Bothe K et al. Uncertainty analysis for the coefficient of band-to-band absorption of crystalline silicon. *AIP Adv* **5**, 067168 (2015).
S40. Kumar A, Rai RC, Podraza NJ, Denev S, Ramirez M et al. Linear and nonlinear optical properties of $BiFeO_3$. *Appl Phys Lett* **92**, 121915 (2008).
S41. Börzsönyi A, Heiner Z, Kalashnikov MP, Kovács AP, Osvay K. Dispersion measurement of inert gases and gas mixtures at 800 nm. *Appl Opt* **47**, 4856–4863 (2008).
S42. Golovashkin AI, Motulevich GP. Optical and electrical properties of Tin. *Sov Phys JETP* **19**, 310–317 (1964).
S43. Zernike F. Refractive indices of ammonium dihydrogen phosphate and potassium dihydrogen phosphate between 2000 Å and 1.5 μ. *J Opt Soc Am* **54**, 1215–1220 (1964).
S44. Ghosh G. Dispersion-equation coefficients for the refractive index and birefringence of calcite and quartz crystals. *Opt Commun* **163**, 95–102 (1999).
S45. Ciesielski A, Skowronski L, Pacuski W, Szoplik T. Permittivity of Ge, Te and Se thin films in the 200–1500 nm spectral range. Predicting the segregation effects in silver. *Mater Sci Semicond Process* **81**, 64–67 (2018).
S46. Bond WL. Measurement of the refractive indices of several crystals. *J Appl Phys* **36**, 1674–1677 (1965).
S47. Malitson IH, Dodge MJ. Refraction and dispersion of lead fluoride. *J Opt Soc Am* **59**, 500A (1969).
S48. Bass M, Van Stryland EW, Williams DR, Wolfe WL. *Handbook of Optics* (McGraw-Hill, New York, 1995).
S49. Bideau-Mehu A, Guern Y, Abjean R, Johannin-Gilles A. Interferometric determination of the refractive index of carbon dioxide in the ultraviolet region. *Opt Commun* **9**, 432–434 (1973).
S50. Singh S, Remeika JP, Potopowicz JR. Nonlinear optical properties of ferroelectric lead Titanate. *Appl Phys Lett* **20**, 135–137 (1972).
S51. Chemnitz M, Gebhardt M, Gaida C, Stutzki F, Kobelke J et al. Hybrid soliton dynamics in liquid-core fibres. *Nat Commun* **8**, 42 (2017).
S52. Gao LH, Lemarchand F, Lequime M. Exploitation of multiple incidences spectrometric measurements for thin film reverse engineering. *Opt Express* **20**, 15734–15751 (2012).
S53. Mishchik K, Ferrer A, de la Cruz AR, Mermillod-Blondin A, Mauclair C et al. Photoinscription domains for ultrafast laser writing of refractive index changes in BK7 borosilicate crown optical glass. *Opt Mater Express* **3**, 67–85 (2013).
S54. https://psec.uchicago.edu/glass/borofloat_33_e.pdf.
S55. Pastrňák J, Roskovcová L. Refraction index measurements on AlN single crystals. *Phys Stat Sol (b)* **14**, K5–K8 (1966).
S56. Sasaki T, Mori Y, Yoshimura M. Progress in the growth of a $CsLiB_6O_{10}$ crystal and its application to ultraviolet light generation. *Opt Mater* **23**, 343–351 (2003).
S57. Lee SY, Jeong TY, Jung S, Yee KJ. Refractive index dispersion of hexagonal boron nitride in the visible and near‐infrared. *Phys Stat Sol (b)* **256**, 1800417 (2019).
S58. Feldman A, Horowitz D. Refractive index of cuprous chloride. *J Opt Soc Am* **59**, 1406–1408 (1969).
S59. Belosludtsev A, Juškevičius K, Ceizaris L, Samuilovas R, Stanionytė S et al. Correlation between stoichiometry and properties of scandium oxide films prepared by reactive magnetron sputtering. *Appl Surf Sci* **427**, 312–318 (2018).
S60. Arakawa ET, Williams MW, Inagaki T. Optical properties of arc‐evaporated carbon films between 0.6 and 3.8 eV. *J Appl Phys* **48**, 3176–3177 (1977).
S61. Boyd G, Kasper H, McFee J. Linear and nonlinear optical properties of $AgGaS_2$, $CuGaS_2$, and $CuInS_2$, and theory of the wedge technique for the measurement of nonlinear coefficients. *IEEE J Quant Elect* **7**, 563–573 (1971).
S62. Vukovic D, Woolsey GA, Scelsi GB. Refractivities of $SF_6$ and $SOF_2$ at wavelengths of 632.99 and 1300 nm. *J Phys D Appl Phys* **29**, 634–637 (1996).
S63. Daimon M, Masumura A. High-accuracy measurements of the refractive index and its temperature coefficient of calcium fluoride in a wide wavelength range from 138 to 2326 nm. *Appl Opt* **41**, 5275–5281 (2002).
S64. Querry MR. Optical constants (Missouri Univ-Kansas City, Kansas City, 1985).
S65. Rodríguez-de Marcos L, Larruquert JI, Aznárez JA, Fernández-Perea M, Soufli R et al. Optical constants of $SrF_2$ thin films in the 25–780-eV spectral range. *J Appl Phys* **113**, 143501 (2013).
S66. Kato K, Umemura N. Sellmeier equations for GaS and GaSe and their applications to the nonlinear optics in $GaS_xSe_{1-x}$. *Opt Lett* **36**, 746–747 (2011).
S67. Weber MJ. *CRC Handbook of Laser Science and Technology Supplement 2*: *Optical Materials* (CRC Press, Boca Raton, 2020).
S68. Treharne RE, Seymour-Pierce A, Durose K, Hutchings K, Roncallo S et al. Optical design and fabrication of fully sputtered CdTe/CdS solar cells. *J Phys Conf Ser* **286**, 012038 (2011).
S69. Ferrini R, Patrini M, Franchi S. Optical functions from 0.02 to 6 eV of $Al_xGa_{1-x}$ Sb/GaSb epitaxial layers. *J Appl Phys* **84**, 4517–4524 (1998).
S70. Uchida N. Optical properties of single-crystal paratellurite ($TeO_2$). *Phys Rev B* **4**, 3736–3745 (1971).
S71. Ninomiya S, Adachi S. Optical properties of cubic and hexagonal CdSe. *J Appl Phys* **78**, 4681–4689 (1995).
S72. Al-Kuhaili MF. Optical properties of hafnium oxide thin films and their application in energy-efficient windows. *Opt Mater* **27**, 383–387 (2004).
S73. Inagaki T, Arakawa ET, Williams MW. Optical properties of liquid mercury. *Phys Rev B* **23**, 5246–5262 (1981).

S74. Kato K, Petrov V, Umemura N. Phase-matching properties of yellow color $HgGa_2S_4$ for SHG and SFG in the 0.944–10.5910 μm range. *Appl Opt* **55**, 3145–3148 (2016).

S75. Pflüger J, Fink J. Determination of optical constants by high-energy, electron-energy-loss spectroscopy (EELS). In *Handbook of Optical Constants of Solids* 293–311 (Elsevier, 1998);https://doi.org/10.1016/B978-0-08-055630-7.50016-X.

S76. Papatryfonos K, Angelova T, Brimont A, Reid B, Guldin S et al. Refractive indices of MBE-grown $Al_xGa_{(1-x)}As$ ternary alloys in the transparent wavelength region. *AIP Adv* **11**, 025327 (2021).

S77. Bond WL, Boyd GD, Carter HL Jr. Refractive indices of HgS (cinnabar) between 0.62 and 11 μ. *J Appl Phys* **38**, 4090–4091 (1967).

S78. Barker AS Jr, Ilegems M. Infrared lattice vibrations and free-electron dispersion in GaN. *Phys Rev B* **7**, 743–750 (1973).

S79. Adachi S. Optical dispersion relations for GaP, GaAs, GaSb, InP, InAs, InSb, $Al_xGa_{1-x}As$, and $In_{1-x}Ga_xAs_yP_{1-y}$. *J Appl Phys* **66**, 6030–6040 (1989).

S80. Ermolaev GA, Yakubovsky DI, Stebunov YV, Arsenin AV, Volkov VS. Spectral ellipsometry of monolayer transition metal dichalcogenides: analysis of excitonic peaks in dispersion. *J Vac Sci Technol B* **38**, 014002 (2020).

S81. Djurišić AB, Li EH, Rakić D, Majewski ML. Modeling the optical properties of AlSb, GaSb, and InSb. *Appl Phys A* **70**, 29–32 (2000).

S82. Gu HG, Song BK, Fang MS, Hong YL, Chen XG et al. Layer-dependent dielectric and optical properties of centimeter-scale 2D $WSe_2$: evolution from a single layer to few layers. *Nanoscale* **11**, 22762–22771 (2019).

S83. Rasigni M, Rasigni G. Optical constants of lithium deposits as determined from the Kramers-Kronig analysis. *J Opt Soc Am* **67**, 54–59 (1977).

S84. Smith NV. Optical constants of sodium and potassium from 0.5 To 4.0 eV by split-beam ellipsometry. *Phys Rev* **183**, 634–644 (1969).

S85. Nigara Y. Measurement of the optical constants of yttrium oxide. *Jpn J Appl Phys* **7**, 404–408 (1968).

S86. Hrabovský J, Kučera M, Paloušová L, Bi L, Veis M. Optical characterization of $Y_3Al_5O_{12}$ and $Lu_3Al_5O_{12}$ single crystals. *Opt Mater Express* **11**, 1218–1223 (2021).

S87. Stephens RE, Malitson IH. Index of refraction of magnesium oxide. *J Res Natl Bur Stand* **49**, 249–252 (1952).

S88. Amotchkina T, Trubetskov M, Hahner D, Pervak V. Characterization of e-beam evaporated Ge, $YbF_3$, ZnS, and $LaF_3$ thin films for laser-oriented coatings. *Appl Opt* **59**, A40–A47 (2020).

S89. Barnes NP, Gettemy DJ. Temperature variation of the refractive indices of yttrium lithium fluoride. *J Opt Soc Am* **70**, 1244–1247 (1980).

S90. Suzuki N, Sawai K, Adachi S. Optical properties of PbSe. *J Appl Phys* **77**, 1249–1255 (1995).

S91. Lomheim TS, DeShazer LG. Optical‐absorption intensities of trivalent neodymium in the uniaxial crystal yttrium orthovanadate. *J Appl Phys* **49**, 5517–5522 (1978).

S92. Luke K, Okawachi Y, Lamont MRE, Gaeta AL, Lipson M. Broadband mid-infrared frequency comb generation in a $Si_3N_4$ microresonator. *Opt Lett* **40**, 4823–4826 (2015).

S93. Larruquert JI, Pérez-Marín AP, García-Cortés S, Rodríguez-de Marcos L, Aznárez JA et al. Self-consistent optical constants of SiC thin films. *J Opt Soc Am A* **28**, 2340–2345 (2011).

S94. Umemura N, Yoshida K, Kato K. Phase-matching properties of $KNbO_3$ in the mid-infrared. *Appl Opt* **38**, 991–994 (1999).